AMERICAN SOCIETY FOR MICROBIOLOGY | mBio

Check for updates

| Virology | Research Article

Exploiting the Affimer platform against influenza A virus

Oliver Debski-Antoniak,[1,2] Alex Flynn,[2,3] David P. Klebl,[2,3] Moisés H. Rojas Rechy,[1,2] Christian Tiede,[1,2] Ian A. Wilson,[4] Stephen P. Muench,[2,3] Darren Tomlinson,[1,2] Juan Fontana[1,2]

AUTHOR AFFILIATIONS See affiliation list on p. 15.

ABSTRACT Influenza A virus (IAV) is well known for its pandemic potential. While current surveillance and vaccination strategies are highly effective, therapeutic approaches are often short-lived due to the high mutation rates of IAV. Recently, monoclonal antibodies (mAbs) have emerged as a promising therapeutic approach, both against current strains and future IAV pandemics. In addition to mAbs, several antibody-like alternatives exist, which aim to improve upon mAbs. Among these, Affimers stand out for their short development time, high expression levels in *Escherichia coli*, and animal-free production. In this study, we utilized the Affimer platform to isolate and produce specific and potent inhibitors of IAV. Using a monomeric version of the IAV trimeric hemagglutinin (HA) fusion protein, we isolated 12 Affimers that inhibit IAV infection *in vitro*. Two of these Affimers were characterized in detail and exhibited nanomolar-binding affinities to the target H3 HA protein, specifically binding to the HA1 head domain. Cryo-electron microscopy (cryo-EM), employing a novel spray approach to prepare cryo-grids, allowed us to image HA-Affimer complexes. Combined with functional assays, we determined that these Affimers inhibit IAV by blocking the interaction of HA with the host-cell receptor, sialic acid. Furthermore, these Affimers inhibited IAV strains closely related to the one used for their isolation. Overall, our results support the use of Affimers as a viable alternative to existing targeted therapies for IAV and highlight their potential as diagnostic reagents.

IMPORTANCE Influenza A virus is one of the few viruses that can cause devastating pandemics. Due to the high mutation rates of this virus, annual vaccination is required, and antivirals are short-lived. Monoclonal antibodies present a promising approach to tackle influenza virus infections but are associated with some limitations. To improve on this strategy, we explored the Affimer platform, which are antibody-like proteins made in bacteria. By performing phage-display against a monomeric version of influenza virus fusion protein, an established viral target, we were able to isolate Affimers that inhibit influenza virus infection *in vitro*. We characterized the mechanism of inhibition of the Affimers by using assays targeting different stages of the viral replication cycle. We additionally characterized HA-Affimer complex structure, using a novel approach to prepare samples for cryo-electron microscopy. Overall, these results show that Affimers are a promising tool against influenza virus infection.

KEYWORDS influenza A virus, Affimer, mAb, cryo-electron microscopy sample preparation

Influenza A virus (IAV) is a paradigmatic virus with pandemic potential. The ability of different IAV strains to recombine and reassort their viral RNA segments to generate a novel strain, enables IAV to undergo dramatic changes in the nature and composition of key proteins in the virus. Combined with its large host range, worldwide zoonotic infection can then ensue (1). Additionally, the error-prone nature of IAV RNA-dependent RNA polymerase enables the virus to further evolve antigenically (2), ultimately resulting

Editor Stephen Turner, Monash University, Clayton, Victoria, Australia

Address correspondence to Juan Fontana, J.Fontana@leeds.ac.uk.

Alex Flynn, David P. Klebl, and Moisés H. Rojas Rechy contributed equally to this article.

The authors declare no conflict of interest.

See the funding table on p. 15.

Received 17 June 2024
Accepted 24 June 2024
Published 22 July 2024

in acquired resistance to licensed antivirals and pre-existing immunity, and the necessity for annual vaccination programmes to maintain immunity in the population, especially the most vulnerable (3). Previous IAV pandemics include the 1918 H1N1 avian pandemic (the Spanish flu), which is estimated to have claimed more than 50 million lives and caused more than 500 million infections worldwide (4), the 1968 H3N2 pandemic, and more recently, the 2009 H1N1 swine flu pandemic (5). Given the mutation rates and the reassortment capacity of IAV, it is likely that further pandemics will occur in the future. For example, both H5N1 and H7N9 of avian origins have been reported to have jumped into humans in multiple instances, with mortalities reported to be as high as 60% and 40%, respectively (6, 7). Due to the nature of these zoonotic outbreaks and their detrimental consequences, improved surveillance combined with a coordinated therapeutic effort will be critical to prevent the impact that future IAV pandemics will have on society.

Neutralizing monoclonal antibodies (mAbs) used as diagnostic and therapeutic approaches are one of the most promising tools for tackling IAV pandemics, in conjunction with annual vaccination campaigns (8). However, mAbs are expensive and often difficult to develop and manufacture, meaning low- and middle-income countries cannot access or afford such therapies (9), thus preventing an effective solution to a global problem. This highlights the need for alternative tools and strategies that can be utilized alongside current treatments to overcome the practical and logistical limitations of mAbs.

Recently, small, synthetic antibody-like proteins termed Affimers have become available as emerging reagents for diagnostics and biotherapeutics (10–12). For example, Affimers have been employed in diagnostic tests for detecting the human-infecting Crimean-Congo hemorrhagic fever virus and the plant-infecting Cowpea Mosaic virus (13, 14) and are actively being developed as oncological therapeutics. Affimer molecules are small (~12 kDa) proteins based on naturally occurring cystatins (cysteine protease inhibitors). These molecules display stability up to high temperatures (~100°C) (12), removing the need for cold chain distribution around the globe. Affimer reagents display two variable peptide regions that allow binding to a target in a similar manner to mAbs, with affinities typically in the low nM range (15). The Affimer randomized variable regions were introduced by PCR. Briefly, a specific oligo-synthesis using trinucleotides for the randomized regions was used to ensure (i) codon-optimized codons for *E. coli*, (ii) even distribution of 19 amino acids except cysteines, and (iii) no stop codons and no stop mutants caused by frameshifts. The high quality of the oligos enabled an overall complexity of 94% and 86.5% after library transformation and phage production, respectively (15). Affimer isolation is performed via phage-display, followed by expression in bacteria. This reduces ethical concerns by removing the need for animals during Affimer development stages and also facilitates rapid, cost-effective, and reproducible production since development times can be reduced from months to just two weeks. Here, we report the first isolation and characterization of Affimer molecules against IAV.

Hemagglutinin (HA), one of the two glycoproteins of IAV, is responsible for virus entry into the host cell. HA comprises two domains: (i) HA1, which includes the N-terminal domain (NTD) and the receptor-binding domain (RBD), is responsible for interaction with host receptors such as sialic acid and for entry into host cells; (ii) HA2, which along with N- and C-termini of HA1 constitutes the fusion domain, is responsible for virus-host cell membrane fusion through conformational changes triggered by the low pH within endocytic compartments that IAV hijacks. In addition to interactions with sialic acid and membrane fusion, HA is also the most abundant glycoprotein in infectious influenza virions and is involved in virus assembly and egress. Due to its multifunctionality, HA is an attractive drug target, as its different functions can be inhibited independently, presenting several target sites on a single viral protein. As such, HA has become a validated therapeutic target (16). However, targeting HA poses many challenges. For example, HA has evolved to support a high degree of mutations resulting from immunogenic pressure. Furthermore, the spike is heavily decorated with glycans,

protecting vulnerable epitopes from antibodies and bulky therapeutics. To date, mAbs have been found that can cross-neutralize group 1 and group 2 influenza viruses (17, 18). For example, the prototypic mAb CR9114 has the capacity to universally recognize group 1 and 2 HA proteins alongside influenza B virus HA spikes (17) although this mAb is not capable of neutralizing all viruses from different strains and subtypes due to the high antigenic variability in the HAs.

Here, we describe the isolation of Affimer molecules specific to the IAV spike protein HA. Two of these Affimers were characterized and found to be potent IAV inhibitors through their binding to the HA RBD and blocking its interaction with its sialic acid receptor. This mechanism of inhibition was further supported by cryo-electron microscopy (cryo-EM) of HA-Affimer complexes. Importantly, we demonstrate that Affimer molecules can inhibit virus efficiently and show their breadth in tackling variants generated through antigenic drift.

RESULTS

Isolation of Affimer molecules against IAV HA

To assess the potential for Affimers as tool compounds against IAV, Affimer molecules were isolated via phage display, expressed in *E. coli*, and characterized (Fig. 1; Fig. S1). Briefly, we immobilized a monomer of the trimeric spike protein HA from the pandemic A/Aichi/68 (H3N2) virus, and a subset of 480 phage clones were selected after three phage-display panning rounds. The individual phages were prepared for initial evaluation. Target binding was carried out via phage enzyme-linked immunosorbent assay (ELISA) (12), and a threshold of >0.5 (absorbance at 620 nm) was employed for selection, resulting in 192 candidates (Fig. S1A). The DNA sequences of the Affimer binders were determined, resulting in 34 unique Affimer sequences (Fig. S1B and S2). None of these Affimers were cytotoxic for tissue-cultured cells when incubated at 100 µM for 72 h (Fig. S1C). A microneutralization assay determined that seven of these Affimers inhibited IAV infection *in vitro* when added to tissue-cultured cells at 3.57 µM (50 µg/mL;

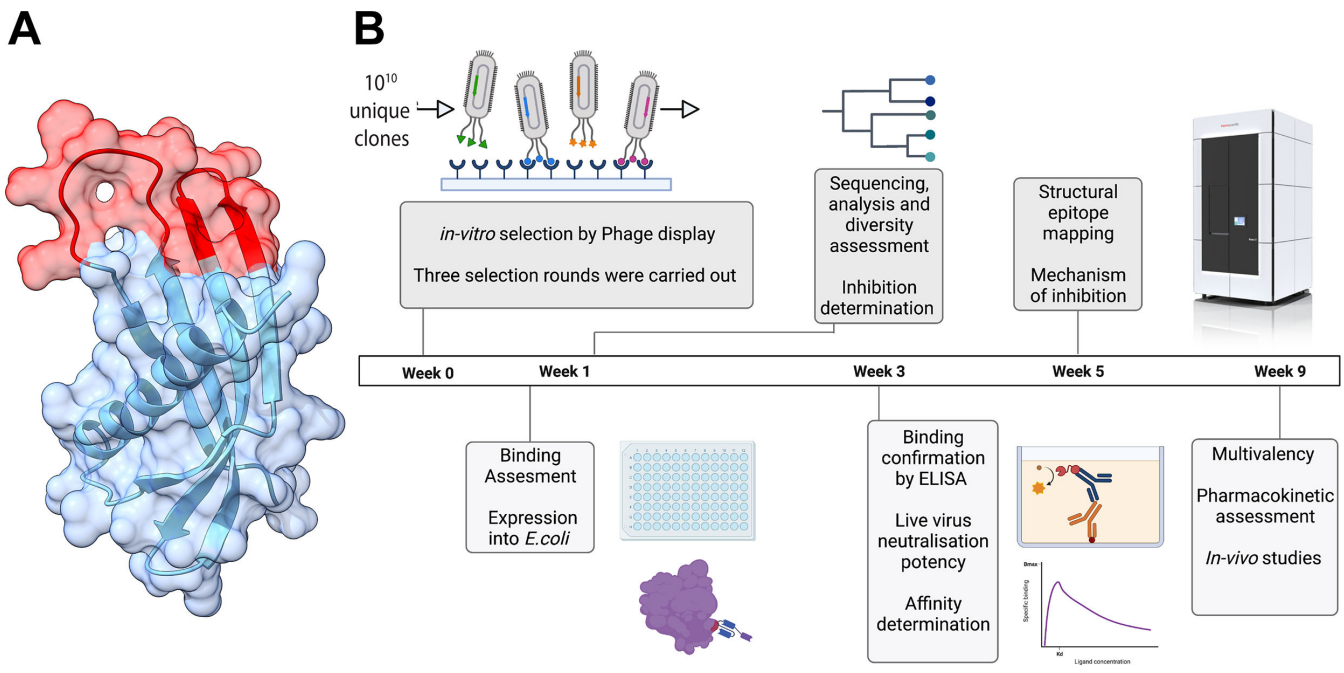

FIG 1 Workflow for isolating and characterizing Affimer molecules against IAV HA. (A) Atomic model of an Affimer molecule overlapped with its surface representation. The two variable peptide regions are highlighted in red. (B) Workflow overview for the generation of anti-IAV Affimer molecules. Top-left to bottom-right schematics represent phage-ELISA, phylogenetic tree, structure determination by cryo-electron microscopy, binding assessment by ELISA, and affinity assessment via ELISA and SPR.

Fig. S1D). Herein, we describe the characterization of two of the promising candidates from this pool: A5 and A31.

Affimer molecules show high affinity against target protein HA

Affimers A5 and A31 were selected due to their high level of neutralization (Fig. S1D) and their high sequence diversity within the neutralizing Affimers, as determined by a phylogenetic tree of the variable region of isolated Affimers (Fig. S2). To determine their binding affinities, surface plasmon resonance (SPR) spectroscopy and ELISAs were employed, again utilizing a monomeric HA [A/Aichi/68 (H3N2)] (Fig. 2). For SPR, Affimer molecules were immobilized onto a streptavidin-coated chip before a range of concentrations of monomeric HA were flowed over the Affimers. A5 and A31 showed Kd values in the low nM range (2.80 ± 1.15 nM for A5 and 5.94 ± 3.27 nM for A31; Fig. 2A and B), demonstrating high-affinity interactions. Both A5 and A31 displayed relatively slow K_{on} association rates (1.15×10^5 M^{-1} s^{-1} for A5 and 2.15×10^4 M^{-1} s^{-1} for A31), but very slow K_{off} rates of dissociation (1.72×10^{-4} s^{-1} for A5 and 1.92×10^{-4} s^{-1} for A31), indicating slow but tight binding of these molecules. Assessment by ELISA further confirmed high-affinity binding to HA. Mean IC_{50} values were calculated by ELISA as 1.01 nM for A5 and 1.06 nM for A31 (Fig. 2C), in the range of the Kd values determined by SPR and comparable to the positive control, the HA-group 2 specific mAb CR8020 (19), which had an IC_{50} value of 0.87 nM. In conclusion, both A5 and A31 bind to their target protein HA with high affinities, comparable to those for mAbs raised against HA, which typically exhibit binding affinities in the range of 0.1 nM–500 nM (20–23).

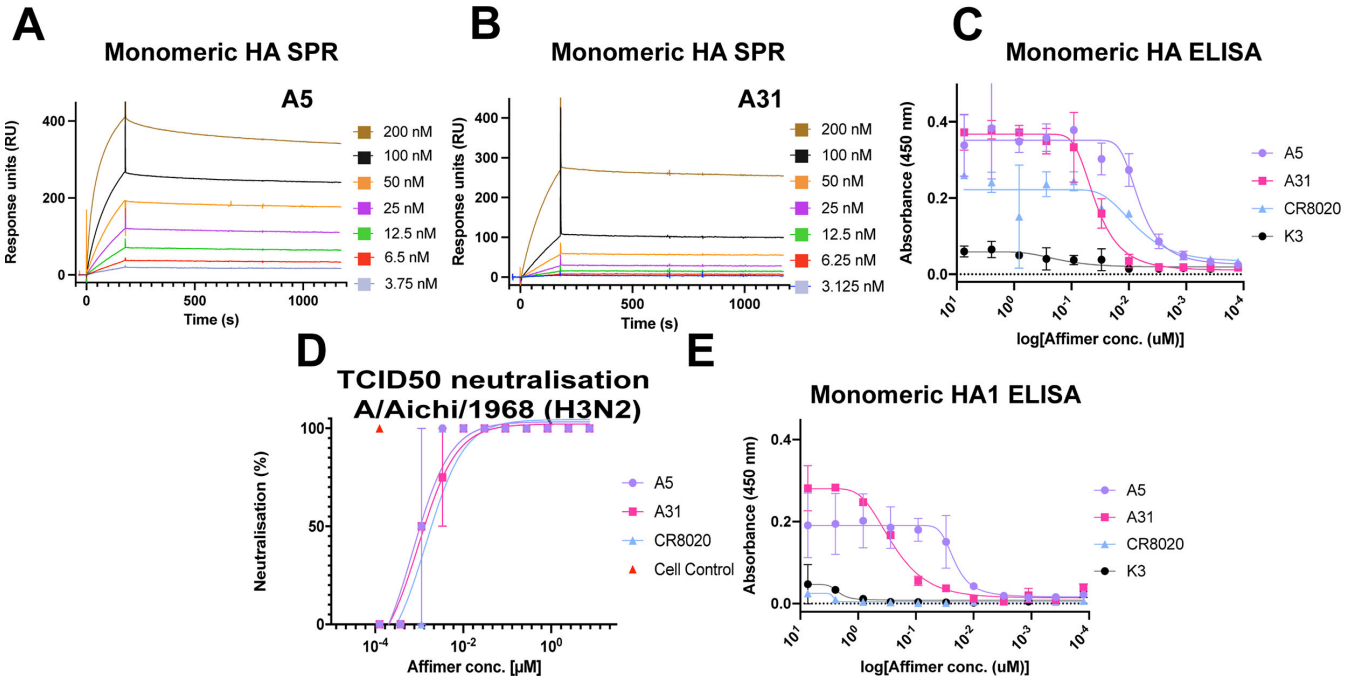

FIG 2 Affimer affinity for IAV monomeric HA and Affimer neutralization efficiency (A, B) Binding of monomeric HA to Affimers as assessed via SPR. HA, in a concentration range (3.75–200 nM), was flown over either immobilized A5 (A) or A31 (B). As monomeric HA was utilized, the HA sensograms were fitted to a Langmuir model, assuming a 1:1 binding interaction. (C) An ELISA was employed as an alternative method to determine the binding affinities of the Affimer molecules to HA. Monomeric [A/Aichi/1968 (H3N2)] HA was absorbed to Maxisorb plates, before a concentration range (7.41 µM–125.5 pM) of biotinylated anti-HA Affimer. A5 (purple circles), A31 (pink squares), mAb CR8020 (blue triangle), or non-specific K3 (black circles); the same color scheme follows throughout. (D) 100× $TCID_{50}$ assay in which A/Aichi/1968 (H3N2) was incubated with A5, A31, or mAb CR8020 in a concentration-dependent manner (7.41 µM–125.5 pM). (E) ELISA to assess binding of A5 or A31 to immobilized HA1 from A/Aichi/1968 (H3N2) (7.41 µM–125.5 pM), including controls mAb CR8020 and Affimer K3. All assays were completed with two biological repeats. In panels C–E, data are mean and error bars represent standard deviation (from two biological repeats, each performed in duplicate).

Affimer molecules show strong potency against IAV through interaction with the receptor-binding site

Once we confirmed that Affimers A5 and A31 bind to HA, we explored their neutralization potency through a $TCID_{50}$ assay against IAV [A/Aichi/1968 (H3N2)]. In this assay, cultured cells were infected with IAV at a concentration that would result in death of the whole monolayer. Affimers were then added to the virus prior to infection in a concentration-dependent manner to monitor inhibition. If Affimers inhibit IAV infection, cells would remain alive, and an intact monolayer would be observed. A5 and A31 both showed comparable, high potency against IAV in the low nM range. The resulting $TCID_{50}$ values were 0.71 nM and 0.96 nM, respectively (Fig. 2D; Fig. S3A), showing comparable potencies to positive control mAb CR8020 at 1.43 nM, which has been shown to broadly neutralize group 2 IAV (19) (24) and other published mAbs (25–27).

To map the epitopes to which both Affimers bind, an ELISA was employed again. In this instance, monomeric HA1, the receptor-binding subunit of HA, was immobilized to wells of a MaxiSorp plate before being incubated with A5, A31, HA2-stem specific CR8020, or non-specific Affimer K3, in a concentration-dependent manner (Fig. 2E). Mean IC_{50} values of 1.05 nM and 0.35 nM, respectively, were obtained for A5 and A31 (Fig. 2E), which are comparable to those observed against full-length HA (Fig. 2C), suggesting that the binding of these Affimer molecules is strictly localized to the HA1 head domain. As expected, the K3 Affimer and mAb CR8020 did not interact with HA1.

To further identify the HA epitopes of A5 and A31, cryo-EM was carried out on each HA-Affimer complex using a trimeric form of HA (HA-HK/68 H3), which has a 98.6% identical sequence to the one HA from A/Aichi/1968 that was used to isolate the Affimers (24). To overcome the preferred orientation of HA observed when grids were prepared using the traditional plunge-freezing vitrification approach (30), we adopted rapid-spray and vitrification for grid preparation (Fig. S4; Table S1) (30, 31), which enabled an H3 HA-only cryo-EM reconstruction at 4.3 Å resolution (Fig. S4A and B; Fig. S5). In addition to a preferred orientation, we noticed that A5 induced HA aggregation when HA-A5 grids were prepared by plunge-freezing. To overcome the on-grid HA aggregation induced by A5, we combined the spray-based grid preparation (27) with rapid mixing (Fig. S4C and D), with the aim of trapping HA after Affimer binding but before aggregation. On the other hand, HA and A31 were pre-incubated for 15 min at room temperature, prior to spraying (Fig. S4E and F). This procedure led to reconstructions of HA in complex with A5 and A31 to global resolutions of 4.4 Å and 3.4 Å, respectively, with imposed C3 symmetry (Fig. 3A and B). The resulting cryo-EM averages confirmed biochemical observations and revealed both A5 and A31 interact either directly with or close to the RBD of HA, potentially obstructing receptor binding and cell entry (Fig. 3A and B). The resolution for the H3-A5 complex was not high enough for accurate model building, likely due to a combination of A5-induced aggregation, preferred orientation, ice-thickness, and limited particle numbers, ultimately leading to strong anisotropy in the map, despite our best efforts to reduce this phenomenon. Rapid mixing reduced aggregation but did not prevent it, reducing the number of particles in a range of orientations available for final reconstructions (23,369 particles for H3-A5 vs 104,544 particles for H3-A31) (Fig. S6 and S7). Furthermore, the resolution estimate for the H3-A5 reconstruction appeared slightly overestimated, preventing atomic modeling. However, the H3-A31 complex was resolved to sufficient resolution to enable model building into the EM density.

The structural and functional basis of HA-A31 interactions

Our two cryo-EM structures showed that both Affimer molecules (A5 and A31) specifically interact with and/or obstruct the RBD of H3 (Fig. 3A and B). The resolution of the H3-A31 average enabled model building and mapping of interactions between A31 and HA. In this model, the two variable peptide regions of A31 appear to straddle the 130-loop of HA (Fig. 4A), which is directly involved in sialic acid binding (Fig. 4B) (32), and suggests that the mechanism of action of A31 (and similarly, of A5), is through competition with receptor binding. The interactions of A31 with HA highlight multiple

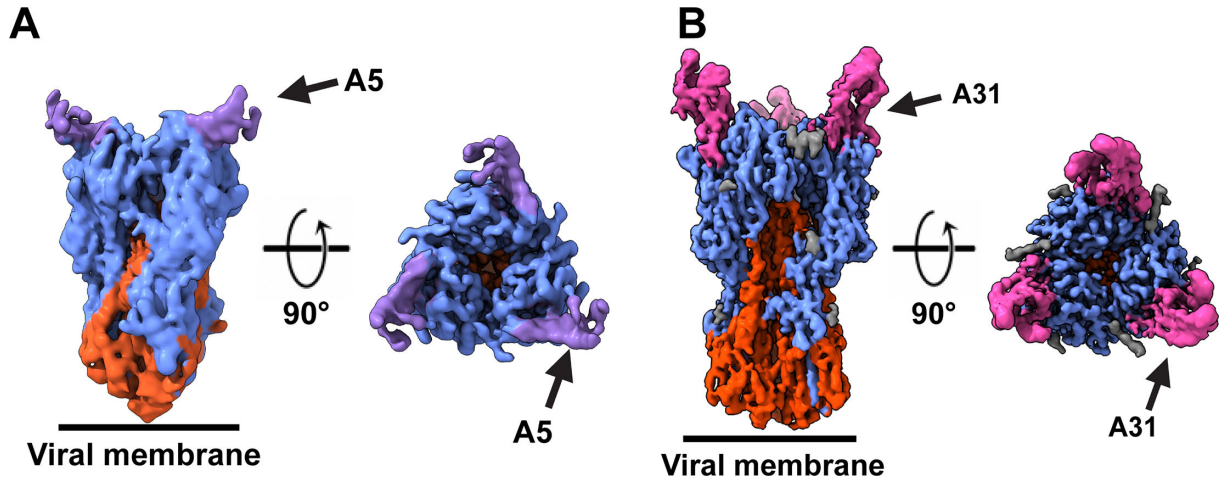

FIG 3 Affimer-HA complex determination by cryo-EM. Cryo-EM maps of the HK68 H3-A5 (A) and HK68 H3-A31 (B). The HK68 H3-A5 map was postprocessed using isonet and local resolution filtered with a sharpening B factor of −20, to reduce anistropic effects (28, 29). HA1 is blue, HA2 is red, A5 is purple, A31 is pink, and glycans are gray.

contact points directly (G135, W153, K156, W222, and S227), or in immediate proximity (R141, G146, R220, and R255) to HA sialic acid interacting residues (Fig. 4A and B) (32).

To confirm the H3-A31 interactions, a panel of H3N2 strains was selected with similar, or distinct residues in the region of H3-A31 interactions. The selected strains included the closely related virus A/Udorn/1972 (H3N2), which exhibits limited adaptions in the sialic acid interaction site [all other residues in this site are identical to A/Aichi/1968 (H3N2) except for G144D, S145I, and T155Y, Fig. 4C]. Additionally, the more recent circulating strains A/Brisbane/2007 (H3N2) and A/Victoria/2011 (H3N2) were selected to provide distinct residues in the receptor-binding region.

Affimer molecules were assessed against these strains using $TCID_{50}$ assays (Fig. 4D and E). A31 maintained high potency, although somewhat decreased, when challenged against A/Udorn/1972 (H3N2) [$TCID_{50}$ of 18.22 nM vs 0.96 nM against A/Aichi/1968 (H3N2); Fig. 4D]. This result could be a consequence of the slight change in the binding pocket due to G144D, S145I, and T155Y mutations (Fig. 4C; Fig. S3B). On the other hand, a decrease in potency was observed when using A5 to neutralize A/Udorn/1972 (H3N2) ($TCID_{50}$ of 3 µM vs 0.71 nM against A/Aichi/1968 (H3N2); Fig. 4E; Fig. S3B). This finding suggests that one or more of the Udorn-specific mutations when compared to Aichi (G144D, S145I, and/or T155Y) are important for A5 binding to HA. When A/Brisbane/2007 (H3N2) and A/Victoria/2011 (H3N2) were challenged with A5 and A31, $TCID_{50}$ values were ≥3 µM, indicating A5 and A31 very weakly inhibit these strains, with the potency being three orders of magnitude lower compared to A/Aichi/1968 (H3N2) (Fig. 4D and E; Fig. S3C and D). Overall, these results validate the cryo-EM observations: as expected from RBD-interacting molecules, both Affimers target a highly variable epitope, and as such lose potency when challenged against different HAs. However, A31 does present some degree of protection against IAV strains closely related to A/Aichi/1968 (H3N2) in terms of their RBD.

Affimers prevent viral entry through interaction with the receptor binding site

HA is the main target of neutralizing antibodies due to its higher abundance compared to NA. Given the different functions of HA during the IAV replication cycle, neutralizing antibodies appear to act by blocking receptor binding, preventing key conformational changes required for successful fusion of viral and cellular membrane, or inhibiting the release of progeny virions (33). Of note, the most potent antibodies typically inhibit receptor binding by blocking the RBD on HA1, while broadly neutralizing antibodies

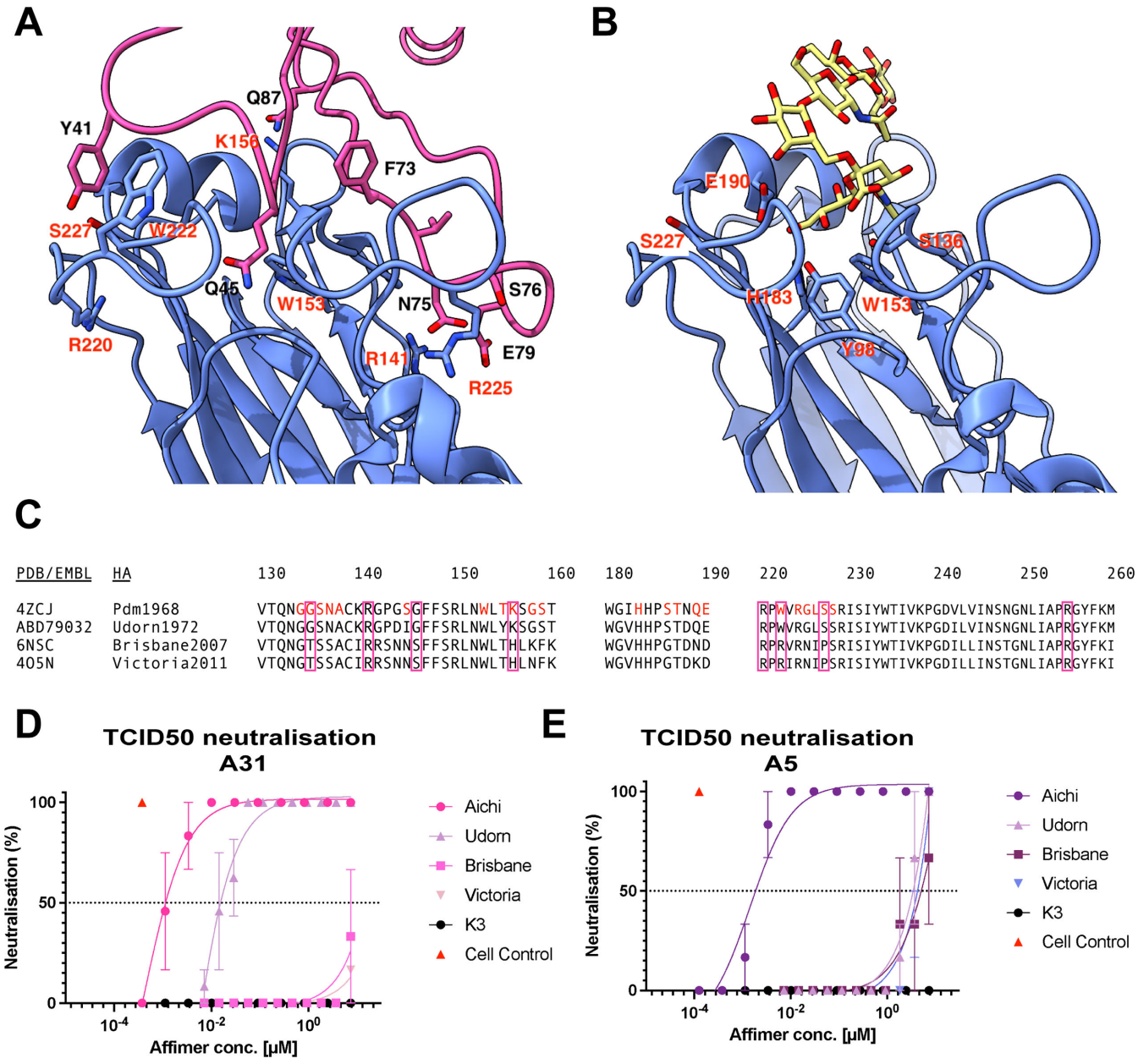

FIG 4 Affimers A5 and A31 target the RBD of A/Aichi/1968 HA and can neutralize related strains. (A) Interacting residues of A31 variable loops with the RBD of HK68 HA. (B) Sialic acid (yellow) docked into the RBD of HA1. Interacting residues with A31 or sialic acid are labeled. (C) Multiple sequence alignment of the RBD of a range of H3N2 viruses. Directly interacting residues with sialic acid for A/Aichi/1968 (H3N2) HA are highlighted in red. Purple boxes show interacting residues with A31. (D, E) 100× $TCID_{50}$ assay in which neutralization of either A31 (D) or A5 (E) was tested against a range of IAV strains in a concentration-dependent manner (7.41 µM–125.5 pM). In panels D and E, data are mean and error bars represent standard deviation (from two biological repeats, each performed in triplicate).

typically target the fusion domain in HA2 (34), although some broadly neutralizing antibodies to the receptor binding site of NA have been recently isolated (35). To further validate RBD binding and to confirm the mechanism of inhibition of A5 and A31, a series of assays were conducted (Fig. S8).

First, to confirm that A5 and A31 inhibit sialic acid binding, a classical IAV hemagglutination inhibition assay was performed (Fig. S8A). In this assay, human red blood cells (RBCs) are incubated with a series of candidates for inhibiting hemagglutination. In the absence of hemagglutination, RBCs accumulate at the bottom of the well, resulting in

a red-colored dot. When IAV alone is added to RBCs, hemagglutination occurs, inducing clumping of RBCs, which no longer accumulate at the bottom of the well, resulting in the absence of a dot. When IAV-induced hemagglutination is blocked, for example due to the presence of an Affimer blocking the interaction with sialic acid, RBCs settle to the bottom of the well resulting in a red dot. When the hemagglutination of IAV A/Aichi/1968 was tested in the presence of A5 and A31, no hemagglutination was detected, even at the lowest concentration tested (223 nM or 3.125 µg/mL; Fig. 5A), confirming previous findings that both Affimer molecules A5 and A31 prevent IAV binding to host cell sialic acids.

We then tested whether A5 and A31 presented additional mechanisms of inhibition, such as blocking fusion or interrupting viral egress. To verify if Affimer molecules inhibited HA fusion, an *in vitro* assay was adapted in which RBCs were incubated on ice with/without IAV to synchronize binding (25) (Fig. S8B). Control or Affimer molecules were then added to RBCs incubated with IAV, before exposing the virus to a fusion buffer (pH 5.0) for 30 min. In the absence of a fusion inhibitor, structural re-arrangements of HA to a post-fusion state induce RBC lysis, causing the release of NADPH, which can be quantified indirectly by an increase in the absorbance at 340 nm. The presence of a fusion inhibitor prevents NADPH from being released to the media and the absorbance at 340 nm does not increase. In the presence of A5 and A31, RBC lysis was also observed, comparable to levels of the non-specific Affimer K3, indicating the Affimer molecules did not inhibit fusion (Fig. 5B).

Finally, we explored if A5 and A31 affected viral egress. In this egress assay, cells were pre-incubated with virus for 4 h, prior to the addition of A5, A31, or control, enabling entry and a single round of infection to occur. Following the addition of Affimer molecules or control, infection was allowed to continue for further 18–20 h, before a hemagglutination assay was carried out. If egress was inhibited, no virions would be present in the media and, therefore, hemagglutination would be observed and RBCs would settle to the bottom of the well (Fig. S8C). Our results showed neither A5 nor A31 inhibited hemagglutination; therefore, they had no effect on viral egress (Fig. 5C). Overall, these results suggest that the mechanism of A5 and A31 inhibition is based solely on their blocking of sialic acid-HA binding by interacting at or around the HA RBD.

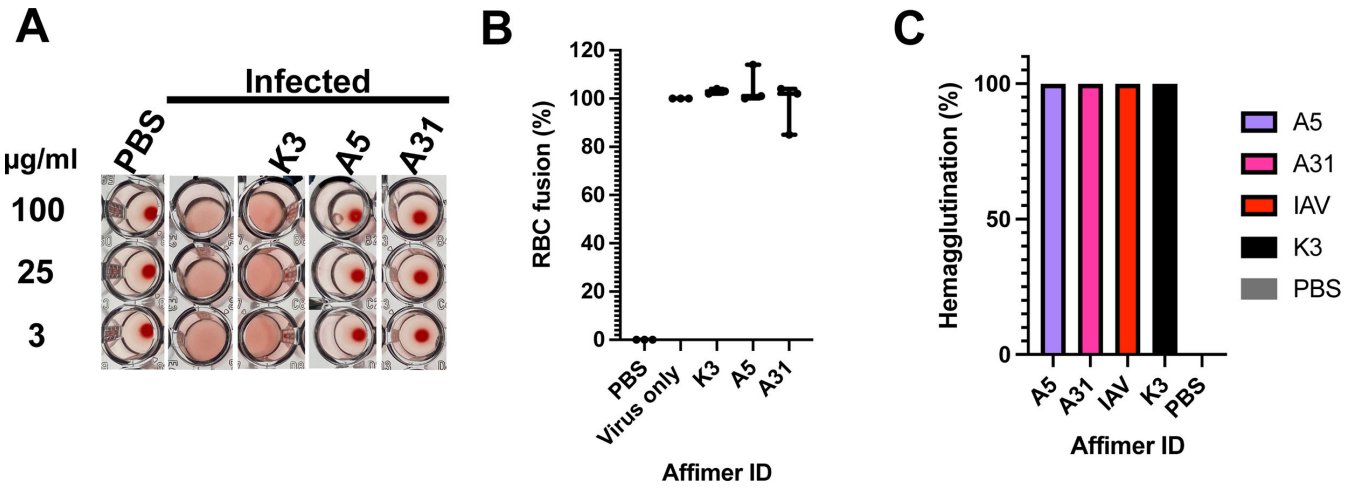

FIG 5 Confirmation of the mechanism of inhibition of A5 and A31. (A) Classical hemagglutination assay in which influenza virus A/Aichi/1968 (H3N2) (4 HA units) was challenged with either A5, A31 or negative control K3 (100, 25, or 3 µg/mL), before adding 1% (vol/vol) hRBC. hRBC incubated with PBS in the absence of virus was used as a positive control for hemagglutination. (B) An adapted fusion assay (25), in which hRBCs were challenged with virus or virus-Affimer complexes and exposed to pH 5 to determine if fusion occurs, as assessed by measuring the release of NAPDH at an absorbance of 340 nm. % fusion was determined by analyzing against virus only control. Data are mean and error bars represent standard deviation (from two biological repeats, each performed in triplicate). (C) An egress assay in which virus infection was synchronized on ice before allowing a single round of infection to occur (4 h). Affimers were then added and infection allowed to continue for a further 18 h before supernatant was used to assess hemagglutination of hRBCs. Two biological repeats were carried out for each assay.

DISCUSSION

To better prepare for future pandemics, multiple strategies are required. Alongside preventive vaccination approaches, mAbs have been favored for therapeutic intervention due to high potency viral neutralization and promising efficacy in animal studies and in the clinic (33). However, due to the nature of pandemic outbreaks, global requirements for rapid manufacturing alongside the cost of production and distribution is a major bottleneck for both vaccines and antibodies (36, 37). Furthermore, resistance rapidly makes therapeutics such as mAbs and antivirals ineffective (3). This highlights the requirement for a variety of interventions, particularly those that can be rapidly and cheaply produced under the threat of emerging pandemic variants. Several alternative therapeutics are under development (38), with some showing success in a clinical setting, such as the DARPin-based Ensovibep, which is in phase II clinical trials directed against SARS-CoV-2 (39). These alternatives, including, for example, nanobodies (40), will likely complement current treatment and perhaps overcome some of the current limitations, such as the disadvantages associated with mAb production and treatment (41).

Here, we showcase the isolation and characterization of Affimer molecules, an alternative to mAbs rapidly being shown to be an effective diagnostic and therapeutic against not only oncological, but more recently viral targets (13–15, 42), as tools against IAV. We carried out a small-scale screen from a library of ~10^{10} Affimer molecules using only the monomeric form of HA (A/Aichi/1968), identifying 34 unique Affimer molecules with different functionalities and binding specificities. Of note, this approach suggests that at least the HA1 domain is correctly folded in monomeric HA, as indicated by the Affimer interaction with HA trimers in the cryo-EM structures. However, it is not known whether the HA2 domain is well-folded in HA monomers although HA monomer structures have been obtained at least for H1N1 HA (43). This work could be, therefore, expanded using trimeric HA molecules for the Affimer screening steps.

The two monovalent Affimer molecules that were characterized in detail here target the RBD, impeding interaction with sialic acid receptors that is necessary for infection of the host cell. We demonstrate that the Affimers not only make high-affinity interactions with HA (K_d < 6 nM) but also show high protection against IAV *in vitro* ($TCID_{50}$ < 1 nM). The affinity of these Affimer molecules for the target protein alongside their potency of virus neutralization is similar to the profile of potent mAbs raised against influenza viruses (20–23, 25–27), for example, mAb CR8020. Since Affimer molecules have already shown good promise as therapeutics, our results pave the way for the use of Affimers as anti-viral therapeutics against IAV in a clinical setting.

However, Affimers A5 and A31 have much lower potency against more recent IAV strains compared to the one that they were screened against. This finding suggests that Affimers A5 and A31 may not be as effective *in vivo* against these strains. One plausible explanation for this reduced inhibition lies in the presence of additional *N*-glycosylation sites, N133 and N144, which were acquired and subsequently maintained through evolutionary processes in all H3N2 strains from 1974 onward (44). Glycosylation at these sites could potentially interfere with the binding affinity and overall effectiveness of A5 and A31 against the A/Brisbane/2007 and A/Victoria/2011 strains of H3N2 influenza since they are situated near the regions where both Affimers interact with HA. Of note, the breadth of some mAbs is based on inserting a single complementarity-determining region into the conserved receptor-binding site, minimizing contact with the surrounding more hypervariable sites (45, 46). A potential way to isolate Affimers targeting only the conserved receptor-binding site would be to perform phage display panning rounds employing HA molecules from different strains, allowing isolation of broad-spectrum Affimers.

Importantly, Affimer molecules have the capacity to overcome many disadvantages that are encountered with therapeutic mAbs. Their small size increases their solubility and rapid tissue penetration, which can often be a setback for mAbs in a clinical setting (41). Affimers typically display a high degree of temperature stability, which might also

enable alternative routes of administration, such as inhalation, as has been described for other highly stable protein scaffolds (47, 48). Furthermore, Affimer molecules lack an Fc-region, likely preventing antibody-dependent enhancement (ADE) effects, a potential side effect of mAbs in patients with inflamed lungs (49), a typical symptom of aggressive respiratory infections (49).

Furthermore, the multimerization of small antibody-like proteins can further enhance individual molecules effectively (39, 50, 51) providing the opportunity to increase avidity for target viral proteins, in the case of same-target multimeric molecules. This approach also provides the potential to improve potency through multimeric molecules targeting multiple immunogenic sites of a viral protein at once, such as the RBD and conserved stem of HA, raising the fitness barrier for escape mutants. To improve half-live, bi-specific Affimer reagents that bind to human serum albumin can also be created, as clearance is an issue for small biologics. We anticipate that the presented workflow for Affimer development could be applied to any future circulatory or more crucially emerging pandemic strain of IAV, and also broadly to other diseases of concern.

The Affimer platform can also be adapted to generate broadly cross-reactive Affimers. To achieve this, a screening protocol with alternating IAV strains within rounds of panning could be employed. For example, Affimers targeting the more highly conserved HA stalk could be isolated following the strategy proposed by Kramer and Palese (51) to induce the production of stalk-reactive antibodies after vaccination. Briefly, they proposed the use of trimeric HA variants or viruses with very similar HA1/HA2 stalk, but divergent HA1 head, so individuals would produce stalk-directed antibodies after sequential exposure to these HA molecules (52). This approach could be easily implemented within the Affimer platform.

Additionally, the Affimers described here could be used as diagnostic tools to detect IAV. Affimers have already been employed for ELISAs to diagnose plant virus diseases (14) and for colorimetric diagnostic tests against Crimean-Congo hemorrhagic fever virus (13). Therefore, broad-spectrum Affimers as described above could be used within these systems to detect viral infection. Furthermore, an Affimer-enzyme-inhibitor switch sensor has been developed (53) that would allow multiplexed detection of respiratory viruses when IAV-specific Affimers are combined with Affimers against other respiratory viruses (e.g., SARS-CoV-2, human respiratory syncytial virus or influenza virus B).

Overall, we have shown that high-affinity and potently neutralizing Affimer molecules can be isolated against influenza A virus, and we have established a workflow to characterize these molecules that could be performed in a matter of weeks, without the requirement of whole antigen, immunization of animals, or access to patient serum. Ultimately, fast-track development strategies of stable and potent inhibitors are critical to raise the global preparedness level toward novel pandemic viruses.

MATERIALS AND METHODS

IAV proteins

The monomeric HA protein employed to select Affimer molecules was a His-tagged monomeric IAV HA derived from A/Aichi/2/1968 (H3N2; SinoBiological Cat: 11707-V08H). To assess affinity through ELISA and SPR, both monomeric HA and HA1 (Cat number 11707-V08H1) from A/Aichi/2/1968 were used (both were His-tagged). For cryo-EM structure determination, a trimeric HA from A/HongKong/1968 was generated and purified as previously described (54).

Cells and viruses

H3N2 IAVs were propagated in MDCK cells including A/Aichi/2/1968 (ATCC VR-1680), A/Udorn/307/1972 (provided by Dr. Lee Sherry, University of Leeds), A/Brisbane/10/2007 (BEI resources, NIAID, NIH: NR-12283), and A/Victoria/361/2011 (BEI resources, NIAID, NIH: NR-44022). Cells were cultured in minimum essential media (MEM, Sigma) supplemented

with 1% FBS and 1× antibiotic antimycotic, which was also supplemented with 10% DMSO.

Selection of HA-specific Affimer molecules by phage display

To select Affimer molecules through phage display, phage libraries were utilized and subjected to three rounds of panning against the monomeric HA protein of A/Aichi/2/1968 (H3N2), as previously described (12). The target protein was immobilized on streptavidin-coated plates, and pre-panned phage was incubated overnight before washing with increasing stringency. Isolated phages were then amplified for phage ELISA.

Screening of isolated Affimer molecules

Phage ELISA screening was performed, as previously described (12), on randomly selected clones from the final panning round of Affimer selection. Screening enabled the positive selection for final evaluation and characterization. To enable a small-scale assessment of IAV-directed Affimer-based therapeutics, an arbitrary cutoff point of >0.5 absorbance reading (at 620 nm) was implemented. Successful candidates were Sanger sequenced and unique Affimers expressed, purified, and characterized.

Affimer production and characterization

After sequencing, the ORFs of unique Affimers were subcloned into a pET11a expression vector. The resultant Affimers were tagged with an N-terminal 8× His-tag and cysteine for functionalization via bacterial expression (*E. coli* strain Rosetta 2). The Affimers were purified using Ni^{2+}-NTA affinity chromatography following previously described methods (12).

Cell viability assay

To determine cell viability, an ATPlite assay was performed following the Perkin Elmer 1-step protocol with slight modifications. Initially, MDCK or A549 cells were seeded in 96-well clear-bottom tissue culture plates at densities of 3×10^4 cells/well and 1.25×10^4 cells/well, respectively, and incubated at 37°C with 5% CO_2 for 24 h. Once the cells reached 80%–90% confluence, the growth medium was removed, and the cells were washed twice with PBS. Next, Affimers at 100 µM (the highest concentration employed for any assay) were added to triplicate wells. All Affimer inhibitors were prepared in infection media. The cells were then incubated at 37°C with 5% CO_2 for 48 h. To measure luminescence, 50 µL of mammalian cell lysis solution was added and incubated on a plate shaker for 5 min, followed by the addition of 50 µL of substrate solution and incubation for a further 5 min. The plate was then dark-adapted, and luminescence was measured at 510 nm using an ELISA plate reader.

Virus neutralization assay

The capacity of Affimer molecules to neutralize viruses was determined by $TCID_{50}$ assay, by crystal violet staining of protected cells in the presence of IAV. Briefly, Affimer candidates were serially diluted from 7.41 µM–125.5 pM in cell culture media (1% FBS-MEM) (in duplicates with three independent repeats). The diluted Affimer candidates or mAb were then exposed to various IAV strains at 100× $TCID_{50}$ in 1% FBS-MEM. Affimer or mAb/virus mixtures were transferred onto 80% confluent MDCK cells. Controls included MDCK cells exposed to Affimer molecules only, cells exposed to virus incubated with a non-IAV specific Affimer (K3; as a negative control), cells exposed to virus incubated with IAV-neutralizing mAb CR8020, cells exposed to virus only (to determine maximal cytopathic effect), and cells incubated with medium only (to determine the baseline state of cells). The plates were incubated for 2–5 days (strain-dependent) at 37°C, and the cytopathic effect was determined by staining with crystal violet solution

(0.5% crystal violet diluted in 37% formaldehyde solution and PBS; all reagents from Sigma Aldrich) for 10 min, followed by washing plates with PBS. Wells were observed for complete protection indicated by an intact blue/violet cell layer, or partial protection in case of ~50% intact cell layer.

Surface plasmon resonance affinity determination of Affimer molecules

Using a Biacore 3000 (GE Healthcare), biotinylated Affimers were immobilized on a Sensor Chip SA (GE Healthcare) through streptavidin-biotin interaction. Affimers were diluted to a concentration of 100 nM in PBS and injected into the respective flow cells at a flow rate of 5 µL/min until the surface density reached 100 response units. A flow cell was left unoccupied as a reference surface. Monomeric HA was diluted in PBS to various concentrations and injected at a flow rate of 20 µL/min for 120 s. BIAevaluation software was employed for double-referencing analysis. Affinity and kinetic constants were determined using a Langmuir 1:1 binding model and steady-state affinity models.

ELISA-based affinity determination of Affimer molecules

Either the monomeric HA or HA1 head domain (both from Aichi and 5 µg/mL per well) were immobilized on Maxisorb plates (Nunc) overnight at 4°C, followed by blocking with 1× casein blocking buffer (Sigma) for 4 h at room temperature. After washing once with PBS, the plates were incubated with a range of concentrations (7.41 µM–125.5 pM) of biotinylated anti-HA Affimer or mAb for 1 h at room temperature. Subsequently, the plate was washed with PBST, and the bound anti-HA Affimer molecules were detected with a 1:1,000 dilution of HRP-conjugated streptavidin (Pierce) for 1 h at room temperature. After washing the plates 10 times with PBST, Affimer molecule binding was visualized with TMB (Seramun) and measured at 450 nm.

Mechanism of inhibition determination by Affimer molecules

The Affimer molecules were serially diluted in PBS in 96-well U-bottom plates at different concentrations (7.41 µM-125.5 pM [in duplicates, three independent repeats]) and exposed to pre-determined-4 HA units of H3N2 (A/Aichi/2/1968) diluted in PBS. After incubating the mixture for 45 min at 37°C, 2% (vol/vol) hRBC (Cambridge Bioscience, RBC1DC4CIT03-XSXX) were added at 1:1 (vol/vol) ratio and incubated at room temperature for 1 h. The hemagglutination effect was then observed visually.

The RBC fusion assay was adapted from previously described methods (25), which involved incubating 1% (vol/vol) hRBC and H3N2 virus (A/Aichi/2/1968) in a 1:1 ratio on ice for 30 min, followed by adding different concentrations of Affimer molecules (7.41 µM, 1.48 µM, 148.15 nM) including a control Affimer (K3). Samples were spun down at 4,000 × *g* for 3 min, supernatant aspirated and 200 µL of buffered solution (15 mM citric acid [pH 5.0], 150 mM $NaCl_2$) before incubating at 37°C for 30 min. Samples were spun at 4,000 × *g* and supernatant harvested and the lysis of RBCs was measured by the presence of NADPH (absorbance at 340 nm).

For the MDCK cell assay, the cells were first infected with an MOI of 5, H3N2 (A/Aichi/2/1968). Affimer molecules or control Affimer K3 were added at 4 h post-infection. At 8 h post-infection, the supernatants were collected, and nascent virus was assessed using a hemagglutination assay.

Cryo-electron microscopy sample preparation of HA

In cryo-EM grid preparation, HA shows strong preferred orientation which can complicate cryo-EM processing (30). We first tested whether our custom-built setup for fast grid preparation would reduce preferred orientation of HA, to enable structure determination of HA in the absence of Affimers and HA-Affimer complexes. A schematic of the setup used for this experiment is given in Fig. S4A. The HA sample was used at 2.9 mg/mL (17.5 µM). Quantifoil 300 mesh copper R1.2/1.3 grids were used after glow discharge in a

Cressington 208 carbon coater with glow-discharge unit for 99 s at 0.1 mbar air pressure and 15 mA.

The sample was injected into a gas-dynamic virtual nozzle made of PDMS (55), at a liquid flowrate of 5.2 µL/s. A spray of the sample was generated by applying an N_2 gas pressure of 2 bar to the nozzle's gas inlet. The spray was allowed to stabilize for 0.8 s, and then the grid was moved through the spray at 1.9 m/s. The distance between spray nozzle and grid was 10 mm at the point of sample application, and the distance between sample application and freezing was 22 mm. This resulted in a residence time of ~12 ms for the sample on the grid. The settings for grid preparation of all samples are summarized in Table S1.

Cryo-electron microscopy of sample preparation HA-A5

For the HA-A5 complex, we modified the setup to allow for rapid mixing and freezing. Previous experiments using pre-mixed HA and Affimer A5 showed aggregated particles that were not amenable to structure determination. Therefore, we chose in-flow mixing with a time delay of 700 ms between mixing of HA and A5 and freezing. The method has been described in detail elsewhere (56), and a schematic of the setup is shown in Fig. S4C. Self-wicking grids supplied by SPT Labtech were used after glow discharge in a Cressington 208 Carbon coater with glow-discharge unit for 80 s at 0.1 mbar air pressure and 15 mA.

The HA sample (5.9 mg/mL, 35 µM) and the A5 sample (1.5× molar excess Affimer A5 and 0.2% octyl glucoside) were loaded into the grid preparation system independently. Mixing of HA and A5 was initiated in a mixing unit upstream of the spray nozzle. The binding reaction took place between the mixing unit and the spray nozzle, in the "delay-line," which was a 20 mm segment of tubing with 381 µm inner diameter. The samples traveled through the system with a combined flowrate of 4.2 µL/s. Assuming laminar flow, this led to a median reaction time of 700 ms. The reaction time for 87% of all particles was between 580 ms and 1,000 ms. The flow through the setup was initiated for 1 s before sample application and plunge-freezing.

Cryo-electron microscopy sample preparation of HA-A31

For the HA-A31 complex, 2.9 mg/mL HA (17.5 µM) was pre-mixed for 15 min at room temperature with 1.5× molar excess of Affimer A31 and 0.1% octyl glucoside, before vitrifying by rapid cryo-EM grid preparation. A schematic of the setup is given in Fig. S4E. Self-wicking grids (SPT Labtech) were used after glow discharge in a Cressington 208 carbon coater with glow-discharge unit for 80 s at 0.1 mbar air pressure and 15 mA.

The sample was injected into a gas-dynamic virtual nozzle made of PDMS (55) at a liquid flowrate of 4.2 µL/s. A spray of the sample was generated by applying an N_2 gas pressure of 2 bar to the nozzle's gas inlet. The spray was allowed to stabilize for 0.8 s, and then the grid was moved through the spray at 1.5 m/s. The distance between spray nozzle and grid was 12 mm at the point of sample application, and the distance between sample application and freezing was 22 mm. This resulted in a residence time of ~15 ms for the sample on the grid.

Cryo-electron microscopy data collection

For HA in the absence of Affimers, movies were collected using a Titan Krios cryo-TEM (Thermo Fisher Scientific) operating at 300 keV and equipped with a K2 Direct Electron Detector (Gatan). Data were acquired using the EPU 2 software (Thermo Fisher Scientific). Movies were collected in electron counting mode at 130,000× corresponding to a calibrated pixel size of 1.07 Å/pix over a defocus range of −3 to −5 µm.

For HA-A5 and HA-A31, movies were collected using a Titan Krios cryo-TEM (Thermo Fisher Scientific) operating at 300 keV and equipped with a Falcon 4 Direct Electron Detector (Thermo Fisher Scientific). Cryo-EM data were acquired using the EPU 2 software (Thermo Fisher Scientific). Movies were collected in electron counting mode,

over a defocus range of −2 to −4 µm and at a nominal magnification of 96,000×, which corresponded to a calibrated pixel size of 0.83 Å/pix.

Cryo-electron microscopy data processing of HA

For the data set of HA in the absence of Affimers, all processing was done in RELION 3.1 (57). Movies were imported and underwent beam-induced motion correction using MotionCor2 (58). Then, the contrast transfer function (CTF) of each micrograph was estimated using gctf (59), crYOLO 1.6.1 was used to automatically pick particles on the motion-corrected micrographs using the weights from its general model and a picking threshold of 0.1. A total of 230,312 particles were picked and extracted into a 280-pixel box re-scaled to 140 pixels. After 2D classification, 151,911 "good" particles were selected. A subset of 50,000 particles was chosen to generate an initial model (with C3 symmetry). This initial model was used for 3D classification of the full set of selected particles with 6 classes over 70 iterations and with C1 symmetry. Particles contributing to the best class (129,501 particles) were reextracted in a 300-pixel box and underwent 3D refinement with C3 symmetry. Two rounds of Bayesian polishing and CTF refinement produced the final structure with a resolution of 4.3 Å.

Cryo-electron microscopy data processing of HA-Affimer complexes

Image processing for both data sets began with the same steps. Movies were imported into RELION 3.1 (57) and underwent beam-induced motion correction using RELION's own implementation (58). Then, the contrast transfer function (CTF) of each micrograph was estimated and corrected for using CTFFIND-4.1 (60). crYOLO 1.6.1 was used to automatically pick particles on the motion corrected micrographs using the weights from its general model and a picking threshold of 0.1. A total of 200,759 particles were picked on the H3-A31 data set and 275, 510 particles were picked on the H3-A5 data set. Particles for both data sets were extracted into a 280-pixel box re-scaled to 100 pixels.

All H3-A5 processing was performed using Relion 3.1. Following extraction, particles underwent one round of 2D classification and the 227,015 particles in the HA-containing classes were taken forward for 3D classification. As only one 3D class contained density for HA with bound Affimers, particles in this class were extracted in a 280-pixel box re-scaled to 200 pixels. These particles were refined with C3 symmetry to generate a map at 5.6 Å resolution. Following two rounds of Bayesian polishing and CTF refinement, the final map with C3 symmetry had a final resolution of 4.4 Å according to the gold standard half-map criteria at a 0.143 cutoff. The final map was postprocessed using isonet and local resolution filtered with a sharpening B factor of −20 (29), to reduce anistropic effects, observed due to orientation bias observed in the data set.

H3-A31 particles were imported into cryoSPARC (61) and underwent one round of 2D classification. Classes containing HA were taken forward for *ab initio* 3D model generation and particles classified into models containing HA were taken back into RELION and re-extracted in a 400-pixel box without re-scaling. The unbinned particles were then processed by cryoSPARC using the algorithm for 3D non-uniform refinement without applied symmetry and then with C3 symmetry. Particles were imported into RELION for Bayesian polishing, then back to cryoSPARC for a second round of non-uniform refinement and global sharpening. This resulted in final map with a global resolution of 3.41 Å according to the gold standard half-map criteria at a 0.143 cut-off.

Overviews of the image processing workflows and statistics are shown in Fig. S5 to S7, and Table S2.

Molecular modeling of H3-A31

AlphaFold models of Affimer molecules A5 and A31 were first generated (28). HK68 (PDB: 4FNK) HA and the Alphafold Affimer models were rigid-body fitted into the cryo-EM maps produced using the UCSF Chimera "fit in map" tool (62). H3-A31 was then modeled by first improving the fit in Coot (63), before utilizing Namdinator (64). To aid model

fitting around the Affimer region, the final H3-A31 map was sharpened using DeepEMhancer (65) as implemented in COSMIC2 (66). This map was used alongside cryoSPARC maps to improve confidence in A31 modeling. The final model was refined in Phenix and iteratively improved in Coot until the model was considered satisfactory. Figures were generated using UCSF Chimera and UCSF ChimeraX (67).

ACKNOWLEDGMENTS

We thank the Astbury Biostructure Laboratory electron microscopy facility, the Protein Interactions facility (Iain Manfield) for support in SPR experiments, Amy Turner from the University of Leeds for support purifying Affimers, and Xueyong Zhu and Chung-Chun D. Lee at The Scripps Research Institute, for providing the trimeric HA protein used in all cryo-EM experiments. Influenza virus strains A/Brisbane/10/2007 and A/Victoria/361/2011 were obtained through BEI Resources, NIAID, NIH (reference numbers NR-12283 and NR-44022).

O.D.-A. was funded by the Rosetrees Trust (A1618) and the University of Leeds. A.F. and D.P.K. were funded by the University of Leeds on the Wellcome Trust 4-year PhD program at the Astbury Centre. M.H.R.R. was funded by CONAHCYT (studentship # 773992). J.F. was funded by the University of Leeds (University Academic Fellow scheme). This work was funded by the Academy of Medical Sciences and the Wellcome Trust (Springboard Award, SBF002\1029) and the Rosetrees Trust (A1618). Electron Microscopy was performed at the Astbury Biostructure Laboratory (University of Leeds), which was funded by the University of Leeds and the Wellcome Trust (108466/Z/15/Z, 090932/Z/09/Z, 221524/Z/20/Z). Partial support was provided by the Bill and Melinda Gates Foundation INV-004923 (I.A.W.).

AUTHOR AFFILIATIONS

[1]School of Molecular and Cellular Biology, Faculty of Biological Sciences, University of Leeds, Leeds, United Kingdom
[2]Astbury Centre for Structural and Molecular Biology, University of Leeds, Leeds, United Kingdom
[3]School of Biomedical Sciences, Faculty of Biological Sciences, University of Leeds, Leeds, United Kingdom
[4]Department of Integrative Structural and Computational Biology, The Scripps Research Institute, La Jolla, California, USA

PRESENT ADDRESS

Oliver Debski-Antoniak, Section Virology, Division Infectious Diseases and Immunology, Department of Biomolecular Health Sciences, Faculty of Veterinary Medicine, Utrecht University, Utrecht, Netherlands
David P. Klebl, Department of Cell and Virus Structure, Max Planck Institute of Biochemistry, Martinsried, Germany

AUTHOR ORCIDs

Oliver Debski-Antoniak http://orcid.org/0000-0001-8239-2738
Juan Fontana http://orcid.org/0000-0002-9084-2927

FUNDING

Funder	Grant(s)	Author(s)
Rosetrees Trust (Rosetrees)	A1618	Oliver Debski-Antoniak
		Juan Fontana

Funder	Grant(s)	Author(s)
Academy of Medical Sciences (The Academy of Medical Sciences)	SBF002\1029	Juan Fontana
University of Leeds	University Academic Fellow scheme	Juan Fontana
Wellcome Trust (WT)	108466/Z/15/Z	Juan Fontana
Wellcome Trust (WT)	090932/Z/09/Z	Juan Fontana
Wellcome Trust (WT)	221524/Z/20/Z	Juan Fontana
Bill and Melinda Gates Foundation (GF)	INV-004923	Ian A. Wilson
Consejo Nacional de Ciencia y Tecnología (CONACYT)	773992	Moisés H. Rojas Rechy

AUTHOR CONTRIBUTIONS

Oliver Debski-Antoniak, Conceptualization, Formal analysis, Investigation, Visualization, Writing – original draft, Writing – review and editing | Alex Flynn, Formal analysis, Investigation, Writing – review and editing | David P. Klebl, Formal analysis, Investigation, Methodology, Writing – review and editing | Christian Tiede, Investigation, Writing – review and editing | Ian A. Wilson, Resources, Writing – review and editing | Stephen P. Muench, Methodology, Supervision, Writing – review and editing | Darren Tomlinson, Conceptualization, Supervision, Writing – review and editing | Juan Fontana, Conceptualization, Funding acquisition, Project administration, Supervision, Writing – original draft, Writing – review and editing.

DATA AVAILABILITY

The cryo-EM maps for H3 HA, H3-A5 and H3-A31 complexes have been deposited in EMDB (accession numbers EMD-18137, EMD-17725 and EMD-17724). The atomic model for the H3-A31 complex has been deposited in the PDB (accession number 8PK3).

ADDITIONAL FILES

The following material is available online.

Supplemental Material

Supplemental Material (mBio01804-24-S0001.pdf). Fig. S1 to S8 and Tables S1 and S2.

REFERENCES

1. Kessler S, Harder TC, Schwemmle M, Ciminski K. 2021. Influenza A viruses and zoonotic events-are we creating our own reservoirs? Viruses 13:2250. https://doi.org/10.3390/v13112250
2. Shao W, Li X, Goraya MU, Wang S, Chen JL. 2017. Evolution of influenza A virus by mutation and re-assortment. Int J Mol Sci 18:1650. https://doi.org/10.3390/ijms18081650
3. Hussain M, Galvin HD, Haw TY, Nutsford AN, Husain M. 2017. Drug resistance in influenza A virus: the epidemiology and management. Infect Drug Resist 10:121–134. https://doi.org/10.2147/IDR.S105473
4. Martini M, Gazzaniga V, Bragazzi NL, Barberis I. 2019. The Spanish influenza pandemic: a lesson from history 100 years after 1918. J Prev Med Hyg 60:E64–E67. https://doi.org/10.15167/2421-4248/jpmh2019.60.1.1205
5. Mena I, Nelson MI, Quezada-Monroy F, Dutta J, Cortes-Fernández R, Lara-Puente JH, Castro-Peralta F, Cunha LF, Trovão NS, Lozano-Dubernard B, Rambaut A, van Bakel H, García-Sastre A. 2016. Origins of the 2009 H1N1 influenza pandemic in swine in Mexico. Edited by R. A. Neher. Elife 5:e16777. https://doi.org/10.7554/eLife.16777
6. Iskander J, Strikas RA, Gensheimer KF, Cox NJ, Redd SC. 2013. Pandemic influenza planning, United States, 1978-2008. Emerg Infect Dis 19:879–885. https://doi.org/10.3201/eid1906.121478
7. Taubenberger JK, Morens DM. 2010. Influenza: the once and future pandemic. Public Health Rep 125 Suppl 3:16–26.
8. Nachbagauer R, Krammer F. 2017. Universal influenza virus vaccines and therapeutic antibodies. Clin Microbiol Infect 23:222–228. https://doi.org/10.1016/j.cmi.2017.02.009
9. Usher AD. 2022. The global COVID-19 treatment divide. Lancet 399:779–782. https://doi.org/10.1016/S0140-6736(22)00372-5
10. Hoffmann T, Stadler LKJ, Busby M, Song Q, Buxton AT, Wagner SD, Davis JJ, Ko Ferrigno P. 2010. Structure-function studies of an engineered scaffold protein derived from stefin A. I: development of the SQM variant. Protein Eng Des Sel 23:403–413. https://doi.org/10.1093/protein/gzq012
11. Stadler LKJ, Hoffmann T, Tomlinson DC, Song Q, Lee T, Busby M, Nyathi Y, Gendra E, Tiede C, Flanagan K, Cockell SJ, Wipat A, Harwood C, Wagner SD, Knowles MA, Davis JJ, Keegan N, Ferrigno PK. 2011. Structure–function studies of an engineered scaffold protein derived

from Stefin A. II: development and applications of the SQT variant. Protein Eng Des Sel 24:751–763. https://doi.org/10.1093/protein/gzr019
12. Tiede C, Tang AAS, Deacon SE, Mandal U, Nettleship JE, Owen RL, George SE, Harrison DJ, Owens RJ, Tomlinson DC, McPherson MJ. 2014. Adhiron: a stable and versatile peptide display scaffold for molecular recognition applications. Protein Eng Des Sel 27:145–155. https://doi.org/10.1093/protein/gzu007
13. Álvarez-Rodríguez B, Tiede C, Hoste ACR, Surtees RA, Trinh CH, Slack GS, Chamberlain J, Hewson R, Fresco A, Sastre P, Tomlinson DC, Millner PA, Edwards TA, Barr JN. 2020. Characterization and applications of a Crimean-Congo hemorrhagic fever virus nucleoprotein-specific Affimer: inhibitory effects in viral replication and development of colorimetric diagnostic tests. PLoS Negl Trop Dis 14:e0008364. https://doi.org/10.1371/journal.pntd.0008364
14. Hesketh EL, Tiede C, Adamson H, Adams TL, Byrne MJ, Meshcheriakova Y, Kruse I, McPherson MJ, Lomonossoff GP, Tomlinson DC, Ranson NA. 2019. Affimer reagents as tools in diagnosing plant virus diseases. Sci Rep 9:7524. https://doi.org/10.1038/s41598-019-43945-6
15. Tiede C, Bedford R, Heseltine SJ, Smith G, Wijetunga I, Ross R, AlQallaf D, Roberts AP, Balls A, Curd A, et al. 2017. Affimer proteins are versatile and renewable affinity reagents. Edited by F. Perez. Elife 6:e24903. https://doi.org/10.7554/eLife.24903
16. Chen Z, Cui Q, Caffrey M, Rong L, Du R. 2021. Small molecule inhibitors of influenza virus entry. Pharmaceuticals (Basel) 14:587. https://doi.org/10.3390/ph14060587
17. Dreyfus C, Laursen NS, Kwaks T, Zuijdgeest D, Khayat R, Ekiert DC, Lee JH, Metlagel Z, Bujny MV, Jongeneelen M, et al. 2012. Highly conserved protective epitopes on influenza B viruses. Science 337:1343–1348. https://doi.org/10.1126/science.1222908
18. Joyce MG, Wheatley AK, Thomas PV, Chuang G-Y, Soto C, Bailer RT, Druz A, Georgiev IS, Gillespie RA, Kanekiyo M, et al. 2016. Vaccine-induced antibodies that neutralize group 1 and group 2 influenza A viruses. Cell 166:609–623. https://doi.org/10.1016/j.cell.2016.06.043
19. Tharakaraman K, Subramanian V, Cain D, Sasisekharan V, Sasisekharan R. 2014. Broadly neutralizing influenza hemagglutinin stem-specific antibody CR8020 targets residues that are prone to escape due to host selection pressure. Cell Host Microbe 15:644–651. https://doi.org/10.1016/j.chom.2014.04.009
20. Bangaru S, Zhang H, Gilchuk IM, Voss TG, Irving RP, Gilchuk P, Matta P, Zhu X, Lang S, Nieusma T, Richt JA, Albrecht RA, Vanderven HA, Bombardi R, Kent SJ, Ward AB, Wilson IA, Crowe JE. 2018. A multifunctional human monoclonal neutralizing antibody that targets a unique conserved epitope on influenza HA. Nat Commun 9:2669. https://doi.org/10.1038/s41467-018-04704-9
21. Kallewaard NL, Corti D, Collins PJ, Neu U, McAuliffe JM, Benjamin E, Wachter-Rosati L, Palmer-Hill FJ, Yuan AQ, Walker PA, et al. 2016. Structure and function analysis of an antibody recognizing all influenza A subtypes. Cell 166:596–608. https://doi.org/10.1016/j.cell.2016.05.073
22. Lee PS, Ohshima N, Stanfield RL, Yu W, Iba Y, Okuno Y, Kurosawa Y, Wilson IA. 2014. Receptor mimicry by antibody F045-092 facilitates universal binding to the H3 subtype of influenza virus. Nat Commun 5:3614. https://doi.org/10.1038/ncomms4614
23. He W, Chen C-J, Mullarkey CE, Hamilton JR, Wong CK, Leon PE, Uccellini MB, Chromikova V, Henry C, Hoffman KW, Lim JK, Wilson PC, Miller MS, Krammer F, Palese P, Tan GS. 2017. Alveolar macrophages are critical for broadly-reactive antibody-mediated protection against influenza A virus in mice. Nat Commun 8:846. https://doi.org/10.1038/s41467-017-00928-3
24. Ekiert DC, Friesen RHE, Bhabha G, Kwaks T, Jongeneelen M, Yu W, Ophorst C, Cox F, Korse H, Brandenburg B, Vogels R, Brakenhoff JPJ, Kompier R, Koldijk MH, Cornelissen L, Poon LLM, Peiris M, Koudstaal W, Wilson IA, Goudsmit J. 2011. A highly conserved neutralizing epitope on group 2 influenza A viruses. Science 333:843–850. https://doi.org/10.1126/science.1204839
25. Wang TT, Tan GS, Hai R, Pica N, Petersen E, Moran TM, Palese P. 2010. Broadly protective monoclonal antibodies against H3 influenza viruses following sequential immunization with different hemagglutinins. PLoS Pathog 6:e1000796. https://doi.org/10.1371/journal.ppat.1000796
26. Iba Y, Fujii Y, Ohshima N, Sumida T, Kubota-Koketsu R, Ikeda M, Wakiyama M, Shirouzu M, Okada J, Okuno Y, Kurosawa Y, Yokoyama S. 2014. Conserved neutralizing epitope at globular head of hemagglutinin in H3N2 influenza viruses. J Virol 88:7130–7144. https://doi.org/10.1128/JVI.00420-14
27. Benjamin E, Wang W, McAuliffe JM, Palmer-Hill FJ, Kallewaard NL, Chen Z, Suzich JA, Blair WS, Jin H, Zhu Q. 2014. A broadly neutralizing human monoclonal antibody directed against a novel conserved epitope on the influenza virus H3 hemagglutinin globular head. J Virol 88:6743–6750. https://doi.org/10.1128/JVI.03562-13
28. Jumper J, Evans R, Pritzel A, Green T, Figurnov M, Ronneberger O, Tunyasuvunakool K, Bates R, Žídek A, Potapenko A, et al. 2021. Highly accurate protein structure prediction with AlphaFold. Nature 596:583–589. https://doi.org/10.1038/s41586-021-03819-2
29. Liu YT, Fan H, Hu JJ, Zhou ZH. 2024. Overcoming the preferred orientation problem in cryoEM with self-supervised deep-learning. bioRxiv:2024.04.11.588921. https://doi.org/10.1101/2024.04.11.588921
30. Tan YZ, Baldwin PR, Davis JH, Williamson JR, Potter CS, Carragher B, Lyumkis D. 2017. Addressing preferred specimen orientation in single-particle cryo-EM through tilting. Nat Methods 14:793–796. https://doi.org/10.1038/nmeth.4347
31. Kontziampasis D, Klebl DP, Iadanza MG, Scarff CA, Kopf F, Sobott F, Monteiro DCF, Trebbin M, Muench SP, White HD. 2019. A cryo-EM grid preparation device for time-resolved structural studies. IUCrJ 6:1024–1031. https://doi.org/10.1107/S2052252519011345
32. Wu NC, Thompson AJ, Xie J, Lin C-W, Nycholat CM, Zhu X, Lerner RA, Paulson JC, Wilson IA. 2018. A complex epistatic network limits the mutational reversibility in the influenza hemagglutinin receptor-binding site. Nat Commun 9:1264. https://doi.org/10.1038/s41467-018-03663-5
33. Brandenburg B, Koudstaal W, Goudsmit J, Klaren V, Tang C, Bujny MV, Korse H, Kwaks T, Otterstrom JJ, Juraszek J, van Oijen AM, Vogels R, Friesen RHE. 2013. Mechanisms of hemagglutinin targeted influenza virus neutralization. PLoS One 8:e80034. https://doi.org/10.1371/journal.pone.0080034
34. Zhang Y, Xu C, Zhang H, Liu GD, Xue C, Cao Y. 2019. Targeting hemagglutinin: approaches for broad protection against the influenza A virus. Viruses 11:405. https://doi.org/10.3390/v11050405
35. Stadlbauer D, Zhu X, McMahon M, Turner JS, Wohlbold TJ, Schmitz AJ, Strohmeier S, Yu W, Nachbagauer R, Mudd PA, Wilson IA, Ellebedy AH, Krammer F. 2019. Broadly protective human antibodies that target the active site of influenza virus neuraminidase. Science 366:499–504. https://doi.org/10.1126/science.aay0678
36. Kelley B. 2020. Developing therapeutic monoclonal antibodies at pandemic pace. Nat Biotechnol 38:540–545. https://doi.org/10.1038/s41587-020-0512-5
37. Watson OJ, Barnsley G, Toor J, Hogan AB, Winskill P, Ghani AC. 2022. Global impact of the first year of COVID-19 vaccination: a mathematical modelling study. Lancet Infect Dis 22:1293–1302. https://doi.org/10.1016/S1473-3099(22)00320-6
38. Vazquez-Lombardi R, Phan TG, Zimmermann C, Lowe D, Jermutus L, Christ D. 2015. Challenges and opportunities for non-antibody scaffold drugs. Drug Discov Today 20:1271–1283. https://doi.org/10.1016/j.drudis.2015.09.004
39. Rothenberger S, Hurdiss DL, Walser M, Malvezzi F, Mayor J, Ryter S, Moreno H, Liechti N, Bosshart A, Iss C, et al. 2022. The trispecific DARPin ensovibep inhibits diverse SARS-CoV-2 variants. Nat Biotechnol 40:1845–1854. https://doi.org/10.1038/s41587-022-01382-3
40. Misson Mindrebo L, Liu H, Ozorowski G, Tran Q, Woehl J, Khalek I, Smith JM, Barman S, Zhao F, Keating C, Limbo O, Verma M, Liu J, Stanfield RL, Zhu X, Turner HL, Sok D, Huang P-S, Burton DR, Ward AB, Wilson IA, Jardine JG. 2023. Fully synthetic platform to rapidly generate tetravalent-bispecific nanobody-based immunoglobulins. Proc Natl Acad Sci U S A 120:e2216612120. https://doi.org/10.1073/pnas.2216612120
41. Chames P, Van Regenmortel M, Weiss E, Baty D. 2009. Therapeutic antibodies: successes, limitations and hopes for the future. Br J Pharmacol 157:220–233. https://doi.org/10.1111/j.1476-5381.2009.00190.x
42. McLaughlin F, Poplawski SE, Sanford DG, Saunders A, Lai JH, Vincent M, Bachovchin WW, Bell N. 2022. AVA6000, a novel precision medicine, targeted to the tumor microenvironment via fibroblast activation protein (FAP) mediated cleavage. Cancer Res 82:1815–1815. https://doi.org/10.1158/1538-7445.AM2022-1815
43. Seok JH, Kim J, Lee DB, Cho KJ, Lee J-H, Bae G, Chung MS, Kim KH. 2017. Conformational modulation of influenza virus hemagglutinin:

characterization and *in vivo* efficacy of monomeric form. Sci Rep 7:7540. https://doi.org/10.1038/s41598-017-08021-x
44. Kobayashi Y, Suzuki Y. 2012. Evidence for N-glycan shielding of antigenic sites during evolution of human influenza A virus hemagglutinin. J Virol 86:3446–3451. https://doi.org/10.1128/JVI.06147-11
45. He W, Mullarkey CE, Duty JA, Moran TM, Palese P, Miller MS. 2015. Broadly neutralizing anti-influenza virus antibodies: enhancement of neutralizing potency in polyclonal mixtures and IgA backbones. J Virol 89:3610–3618. https://doi.org/10.1128/JVI.03099-14
46. Whittle JRR, Zhang R, Khurana S, King LR, Manischewitz J, Golding H, Dormitzer PR, Haynes BF, Walter EB, Moody MA, Kepler TB, Liao H-X, Harrison SC. 2011. Broadly neutralizing human antibody that recognizes the receptor-binding pocket of influenza virus hemagglutinin. Proc Natl Acad Sci U S A 108:14216–14221. https://doi.org/10.1073/pnas.1111497108
47. Schilling J, Jost C, Ilie IM, Schnabl J, Buechi O, Eapen RS, Truffer R, Caflisch A, Forrer P. 2022. Thermostable designed ankyrin repeat proteins (DARPins) as building blocks for innovative drugs. J Biol Chem 298:101403. https://doi.org/10.1016/j.jbc.2021.101403
48. He S, Gui J, Xiong K, Chen M, Gao H, Fu Y. 2022. A roadmap to pulmonary delivery strategies for the treatment of infectious lung diseases. J Nanobiotechnology 20:101. https://doi.org/10.1186/s12951-022-01307-x
49. Bournazos S, Gupta A, Ravetch JV. 2020. The role of IgG Fc receptors in antibody-dependent enhancement. Nat Rev Immunol 20:633–643. https://doi.org/10.1038/s41577-020-00410-0
50. Hanke L, Das H, Sheward DJ, Perez Vidakovics L, Urgard E, Moliner-Morro A, Kim C, Karl V, Pankow A, Smith NL, Porebski B, Fernandez-Capetillo O, Sezgin E, Pedersen GK, Coquet JM, Hällberg BM, Murrell B, McInerney GM. 2022. A bispecific monomeric nanobody induces spike trimer dimers and neutralizes SARS-CoV-2 *in vivo*. Nat Commun 13:155. https://doi.org/10.1038/s41467-021-27610-z
51. Krammer F, Palese P. 2013. Influenza virus hemagglutinin stalk-based antibodies and vaccines. Curr Opin Virol 3:521–530. https://doi.org/10.1016/j.coviro.2013.07.007
52. Nachbagauer R, Feser J, Naficy A, Bernstein DI, Guptill J, Walter EB, Berlanda-Scorza F, Stadlbauer D, Wilson PC, Aydillo T, et al. 2021. A chimeric hemagglutinin-based universal influenza virus vaccine approach induces broad and long-lasting immunity in a randomized, placebo-controlled phase I trial. Nat Med 27:106–114. https://doi.org/10.1038/s41591-020-1118-7
53. Adamson H, Ajayi MO, Campbell E, Brachi E, Tiede C, Tang AA, Adams TL, Ford R, Davidson A, Johnson M, McPherson MJ, Tomlinson DC, Jeuken LJC. 2019. Affimer–enzyme–inhibitor switch sensor for rapid wash-free assays of multimeric proteins. ACS Sens 4:3014–3022. https://doi.org/10.1021/acssensors.9b01574
54. Ekiert DC, Kashyap AK, Steel J, Rubrum A, Bhabha G, Khayat R, Lee JH, Dillon MA, O'Neil RE, Faynboym AM, Horowitz M, Horowitz L, Ward AB, Palese P, Webby R, Lerner RA, Bhatt RR, Wilson IA. 2012. Cross-neutralization of influenza A viruses mediated by a single antibody loop. Nature 489:526–532. https://doi.org/10.1038/nature11414
55. Klebl DP, Monteiro DCF, Kontziampasis D, Kopf F, Sobott F, White HD, Trebbin M, Muench SP. 2020. Sample deposition onto cryo-EM grids: from sprays to jets and back. Acta Crystallogr D Struct Biol 76:340–349. https://doi.org/10.1107/S2059798320002958
56. Klebl DP, White HD, Sobott F, Muench SP. 2021. On-grid and in-flow mixing for time-resolved cryo-EM. Acta Crystallogr D Struct Biol 77:1233–1240. https://doi.org/10.1107/S2059798321008810
57. Zivanov J, Nakane T, Scheres SHW. 2020. Estimation of high-order aberrations and anisotropic magnification from cryo-EM data sets in RELION-3.1. IUCrJ 7:253–267. https://doi.org/10.1107/-S2052252520000081
58. Zheng SQ, Palovcak E, Armache JP, Verba KA, Cheng Y, Agard DA. 2017. MotionCor2:anisotropic correction of beam-induced motion for improved cryo-electron microscopy. Nat Methods 14:331–332. https://doi.org/10.1038/nmeth.4193
59. Zhang K. 2016. Gctf: real-time CTF determination and correction. J Struct Biol 193:1–12. https://doi.org/10.1016/j.jsb.2015.11.003
60. Rohou A, Grigorieff N. 2015. CTFFIND4: fast and accurate defocus estimation from electron micrographs. J Struct Biol 192:216–221. https://doi.org/10.1016/j.jsb.2015.08.008
61. Punjani A, Rubinstein JL, Fleet DJ, Brubaker MA. 2017. cryoSPARC: algorithms for rapid unsupervised cryo-EM structure determination. Nat Methods 14:290–296. https://doi.org/10.1038/nmeth.4169
62. Pettersen EF, Goddard TD, Huang CC, Couch GS, Greenblatt DM, Meng EC, Ferrin TE. 2004. UCSF Chimera—a visualization system for exploratory research and analysis. J Comput Chem 25:1605–1612. https://doi.org/10.1002/jcc.20084
63. Emsley P, Lohkamp B, Scott WG, Cowtan K. 2010. Features and development of *Coot*. Acta Crystallogr D Biol Crystallogr 66:486–501. https://doi.org/10.1107/S0907444910007493
64. Kidmose RT, Juhl J, Nissen P, Boesen T, Karlsen JL, Pedersen BP. 2019. Namdinator - automatic molecular dynamics flexible fitting of structural models into cryo-EM and crystallography experimental maps. IUCrJ 6:526–531. https://doi.org/10.1107/S2052252519007619
65. Sanchez-Garcia R, Gomez-Blanco J, Cuervo A, Carazo JM, Sorzano COS, Vargas J. 2021. DeepEMhancer: a deep learning solution for cryo-EM volume post-processing. Commun Biol 4:874. https://doi.org/10.1038/s42003-021-02399-1
66. Cianfrocco MA, Wong-Barnum M, Youn C, Wagner R, Leschziner A. 2017. Cosmic2: a science gateway for cryo-electron microscopy structure determination. Proceedings of the Practice and Experience in Advanced Research Computing 2017 on Sustainability, Success and Impact (PEARC17). Association for Computing Machinery, New York, NY, USA. https://doi.org/10.1145/3093338.3093390
67. Goddard TD, Huang CC, Meng EC, Pettersen EF, Couch GS, Morris JH, Ferrin TE. 2018. UCSF ChimeraX: meeting modern challenges in visualization and analysis. Protein Sci 27:14–25. https://doi.org/10.1002/pro.3235